

See discussions, stats, and author profiles for this publication at: <https://www.researchgate.net/publication/256663611>

Coherent Exciton Delocalization in Strongly Coupled Quantum Dot Arrays

ARTICLE *in* NANO LETTERS · SEPTEMBER 2013

Impact Factor: 13.59 · DOI: 10.1021/nl402725m · Source: PubMed

CITATIONS

12

READS

47

5 AUTHORS, INCLUDING:



[Joel N Schrauben](#)

National Renewable Energy Laboratory

11 PUBLICATIONS 224 CITATIONS

[SEE PROFILE](#)



[Matthew C Beard](#)

National Renewable Energy Laboratory

114 PUBLICATIONS 7,874 CITATIONS

[SEE PROFILE](#)



[Joseph M Luther](#)

National Renewable Energy Laboratory

83 PUBLICATIONS 5,246 CITATIONS

[SEE PROFILE](#)



[Justin C Johnson](#)

National Renewable Energy Laboratory

75 PUBLICATIONS 11,836 CITATIONS

[SEE PROFILE](#)

Coherent Exciton Delocalization in Strongly Coupled Quantum Dot Arrays

Ryan W. Crisp,^{†,‡} Joel N. Schrauben,[†] Matthew C. Beard,[†] Joseph M. Luther,[†] and Justin C. Johnson*,^{†,‡}

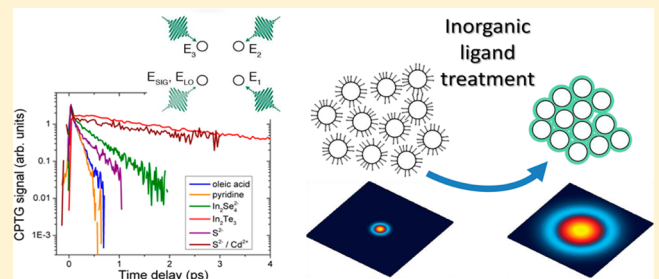
[†]National Renewable Energy Laboratory, 15013 Denver West Pkwy, Golden, Colorado 80401, United States

[‡]Department of Physics, Colorado School of Mines, Golden, Colorado 80401, United States

S Supporting Information

ABSTRACT: Quantum dots (QDs) coupled into disordered arrays have exhibited the intriguing property of bulk-like transport while maintaining discrete excitonic optical transitions. We have utilized ultrafast cross-polarized transient grating (CPTG) spectroscopy to measure electron–hole wave function overlap in CdSe QD films with chemically modified surfaces for tuning inter-QD electronic coupling. By comparing the CPTG decays with those of isolated QDs, we find that excitons coherently delocalize to form excited states more than 200% larger than the QD diameter.

KEYWORDS: Quantum dot, nonlinear, ultrafast, exciton, spin, delocalization



Electronic excitations in isolated quantum dots (QDs) are constrained by the physical size of the nanostructure and thus display a manifold of exciton states derived from confinement of the band structure of the material by an infinite spherical potential of well-defined diameter.^{1,2} Reduction in interparticle distance and the type or amount of material between QDs in a film can incite wave function expansion beyond the QD boundary, thus perturbing the isolated QD exciton state manifold. This perturbation in excited state electronic structure, which is inevitable in almost all practical schemes of solar photoconversion involving colloidal QDs, is bound to influence photophysical properties that have been studied in detail only for isolated nanostructures. For example, multiexciton processes like multiple exciton generation (MEG)³ and Auger decay⁴ depend on electron–hole Coulomb interactions that scale inversely with the effective size of the exciton. Moreover, the rate of thermal equilibration of carriers after photoexcitation in hot carrier extraction schemes may depend on the effective exciton size.⁵ It is therefore crucial to measure quantitatively the exciton size after photoexcitation, which is the initial condition for all subsequent dynamics.

The extent of the excited state wave function perturbation induced by close QD coupling is not trivial to isolate experimentally, as many material properties also exhibit continuous variation in behavior as the bulk limit is approached. During the past several years, researchers have reported on a large number of successful ligand exchange and surface manipulation treatments for creating electronically coupled nanocrystal arrays.⁶ Short-chain organic ligands,⁷ inorganic salts,⁸ and metal chalcogenide complex (MCC) ligands⁹ have increased charge carrier mobilities in close-packed films fabricated from surface-modified colloidal QDs compared to those retaining the native organic ligands from synthesis.

Photophysically, these treatments produce a broadened and red-shifted, yet still distinct, lowest exciton absorption feature. Charge carrier mobilities in such films, determined by time-resolved microwave conductivity (TRMC) measurements or measuring the gate response of the array in a field-effect transistor (FET), have exceeded $10 \text{ cm}^2 \text{ V}^{-1} \text{ s}^{-1}$ for PbSe QDs¹⁰ and CdSe QDs.¹¹ Even in the absence of long-range order, transport was found to occur without thermal activation, implying a change from a charge hopping transport mechanism to a regime that is more coherent or band-like. While true band transport (i.e., fully delocalized states) across a macroscopic film seems unlikely in such samples,¹² coherent expansion of excited states over shorter ranges remains possible and could lead to the observed temperature dependence.^{13,14} Neither TRMC nor FET measurements report directly on exciton delocalization since each is sensitive only to free charges, but these interesting observations may have at their origin the presence of a delocalized exciton state that is less sensitive to typical activation barriers to percolation and more efficiently moves charge over long distances.

In this Letter we investigate the ultrafast transition from localized and quantum-confined excitons created by photoabsorption in coupled CdSe QD films to delocalized excitons extending over multiple QDs. We find that the MCC ligand In₂Te₃ produces the largest effective exciton size without thermal annealing, about 2.2 times the known QD size. Mild thermal annealing of pyridine-capped QDs also produces a significantly larger exciton size, but the onset of necking or sintering at higher temperatures eventually destroys the

Received: July 23, 2013

Revised: August 29, 2013

Published: September 16, 2013



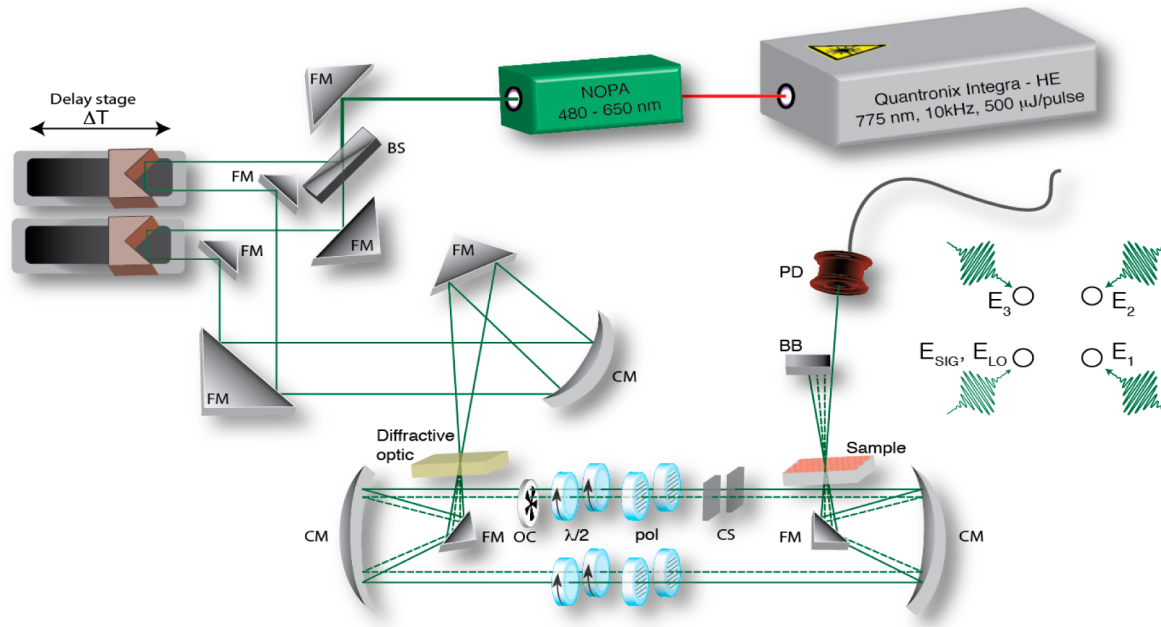


Figure 1. Experimental setup for cross-polarized transient grating spectroscopy. FM = folding mirror, BS = beamsplitter, CM = curved mirror, OC = optical chopper, CS = coverslip, BB = beam block, PD = photodiode, $\lambda/2$ = half waveplate.

simultaneous presence of quantum confinement and delocalization. We explore the consequences of these findings for secondary and tertiary events like Auger recombination and charge conduction.

Cross-polarized transient grating spectroscopy (CPTG) has been proven as a viable means by which to measure coherent exciton delocalization in isolated QDs in advance of other excited state processes,^{15–17} thus providing a “snapshot” of the effective exciton size. CPTG is a four-wave mixing process, depicted in Figure 1, in which two coincident ultrafast pulses with orthogonal polarizations and slightly different k -vectors interact on a sample to produce a spatially varying modulation of the phase of the photoexcited excitons.¹⁸ Exciton fine structure relaxation (i.e., spin flipping) alters the phase grating during the waiting period for the third pulse, even while the overall excited state population remains constant. When the detected polarization is orthogonal to that of the third pulse, the signal amplitude depends on the phase change that results from a flipped spin. Destructive interference between flipped and unflipped exciton contributions leads to signal decay, leaving CPTG as a measure of specifically coherent dynamics.

Briefly, a home-built noncollinear parametric amplifier (NOPA) operating at 10 kHz was tuned to the peak of the lowest exciton absorption and compressed to approximately 30 fs width, measured by autocorrelation in a 50 μm thick BBO crystal at the sample position (Figure S2). The full NOPA output pulse energy prior to entering the interferometers was approximately 100 nJ. The beam was then split evenly into two copies using an ultrathin beamsplitter, with each beam traversing a delay stage before being focused into a diffractive optic (DO, Holoeye). The DO was optimized for +1 and -1 order diffraction, producing identical copies of each beam translated horizontally. k_1 and k_2 remained time-overlapped, with their delay from the k_3/k_4 pulse pair controlled by a motorized delay stage. The four beams then propagated parallel paths in a boxcar configuration, each through a $\lambda/2$ waveplate and polarizer combination before being focused into the sample

to a common spot using an 8 in. focal length spherical Ag mirror. Glass coverslips were inserted in the paths of k_3 and k_4 , the latter of which contained varying thicknesses of evaporated silver, and mounted on a rotation stage. k_4 is identified as the local oscillator (LO) in the heterodyne detection scheme, with its phase and power accurately controlled to produce the desired signal. k_3 was chopped at 3.3 kHz to provide a frequency for lock-in detection. The beam size at the sample was approximately 230 μm , with the pulse energy in each beam set at about 5 nJ. A mask blocked beams coming from the sample except in the direction of k_4 , where a set of irises was used to reject scattering and define the signal beam path. The copropagating signal and LO were focused onto the same spot on a Si photodiode. Using the pump intensity and known absorption cross section for CdSe QDs,¹⁹ we determined the average exciton occupation $\langle N_{\text{eh}} \rangle$ following each pulse to be no higher than 0.02, indicating that experiments were performed in a highly dilute excitation regime. Higher order or thermal effects are also ruled out as experiments were performed in a regime where the kinetics were independent of pump fluence. The measured CPTG signal is actually a convolution between the population decay and the fine structure relaxation. Pump-probe measurements described below and common polarization TG scans did not contain decay components faster than about 10 ps, much shorter than the CPTG decay window; thus the deconvolution was deemed unnecessary (Figure S3).

The exciton levels that make up the fine structure are labeled by their total angular momentum F and are split from each other by exchange and crystal anisotropy effects, yielding a manifold of levels with $F = +, -, 0$ spanning an energy range of several to tens of meV.² Both exchange and spin-orbit effects that mediate the transition between fine structure levels are dependent on electron-hole overlap and thus the size of the exciton. The CPTG decay rate constant, k_{CPTG} , is related to the splitting between relevant levels by Fermi's Golden rule. Since CPTG decays have been measured in isolated QDs of known size, an effective “ruler” of k_{CPTG} vs exciton size is known

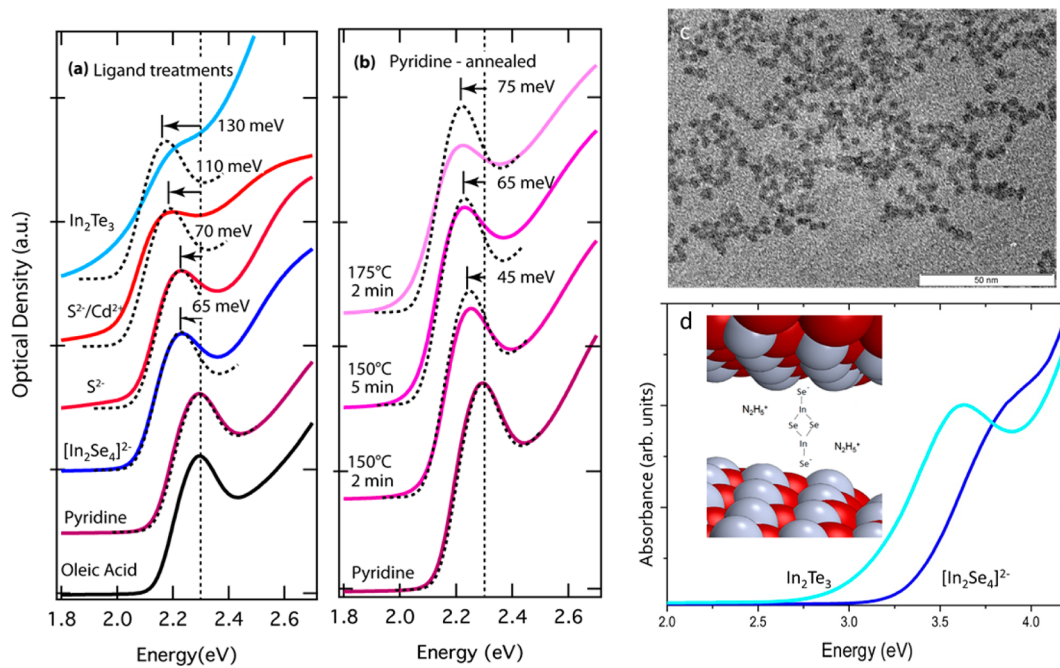


Figure 2. Absorption spectra of the CdSe QD films studied here. (a) Various chemical treatments for ligand replacement and (b) pyridine treatment followed by thermal annealing (temperature and time noted). The spectra are vertically offset for clarity. A shifted copy of the as-cast film spectrum with OA ligands is shown as dashed lines, where the red-shifted energy needed to align the peaks is noted for each trace. The vertical dashed line is the peak position of the uncoupled QD 1S exciton. (c) TEM of pyridine-exchanged QDs, showing preferential chain formation. (d) Absorption spectra of $[\text{In}_2\text{Se}_4]^{2-}$ and In_2Te_3 ligands in hydrazine solution. Inset: Bonding scheme for MCC ligands at the QD surface, with counterbalancing hydrazinium ions.

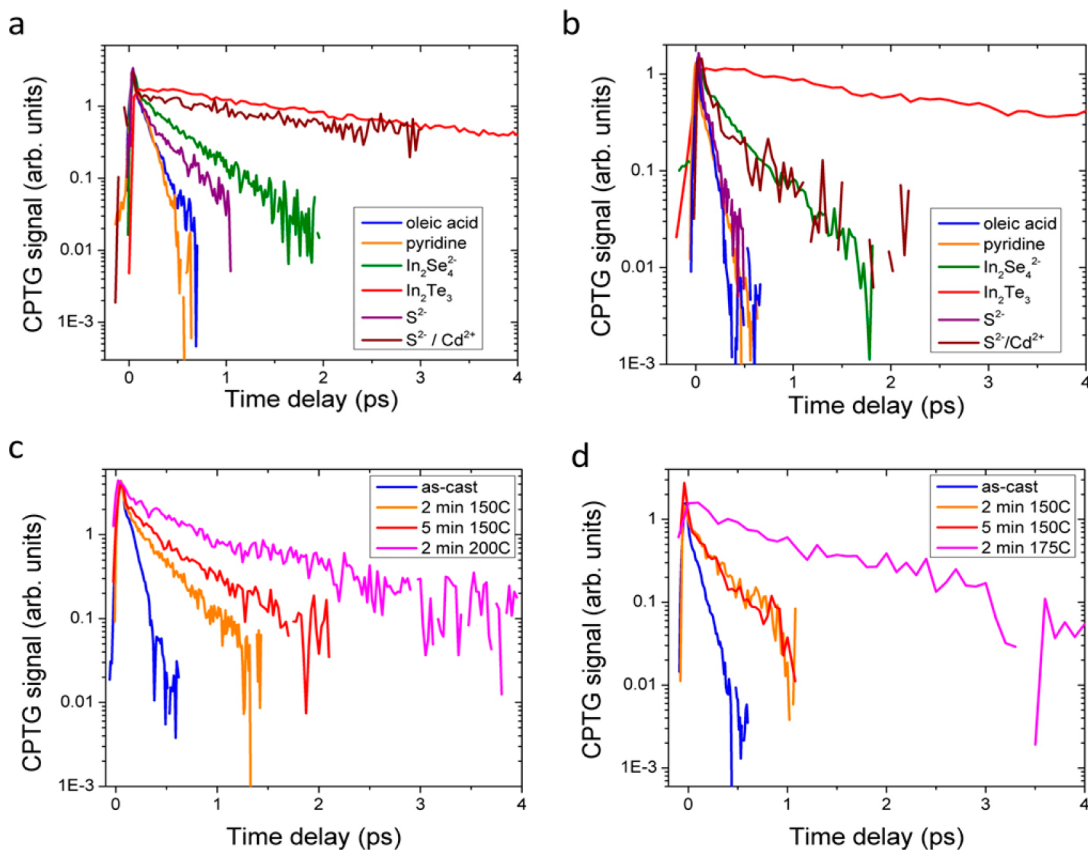


Figure 3. Cross-polarized transient grating decay traces vs surface ligand treatment. Films are drop-cast from (a,c) 3.0 nm and (b,d) 2.8 nm CdSe QDs. Parts c and d are pyridine-treated followed by thermal annealing.

($k_{\text{CPTG}} \propto 1/d^4$ for CdSe).¹⁶ We can then use this ruler to measure the degree of exciton delocalization in QD films treated by various methods known to produce good performance in optoelectronic devices.

The MCC ligands were synthesized and exchanges performed on either oleate or TOPO capped QDs, similar to Kovalenko et al.⁹ The synthesis and exchange with Na₂S was carried out in a similar manner to Nag et al.⁸ For the inorganic ligands the substrates were heated to 60 °C as the solutions were dropcast. Other films were drop cast onto 0.5 mm thick sapphire substrates at room temperature from either 9:1 hexane–octane or 4:1 chloroform–pyridine solutions. The Cd²⁺ metal ion treatment on the Na₂S film was performed as in Nag et al.²⁰ All films were sealed in inert atmosphere by placing the film between two sapphire windows with an intervening O-ring.

In Figure 2a,b we display the extinction spectra of the various QD films studied here. We have analyzed our data near the lowest exciton band by overlaying a red-shifted copy of the spectrum from the oleic acid (OA)-capped QDs. We observe four effects on the optical properties after ligand-treatments or thermal-annealing: (1) red-shift of the 1S exciton feature; (2) broadening of the 1S exciton feature; (3) a low energy tail; and (4) changes on the high-energy side of the spectrum.

There have been many reports concerning the modification of the optical properties of QDs upon film formation and subsequent QD–QD electronic coupling. Micic and co-workers²¹ studied the optical properties of InP QD films where the QD separation was varied by exchanging ligands of different length prior to film formation. They observed a broadening and redshift of the lowest exciton band that depended on the QD size and ligand length, ascribing the 140 meV redshift to quantum mechanical coupling. A similar shift was observed in films prepared from CdSe clusters but interpreted as a change in the polarization energy rather than quantum mechanical coupling.²² A 1D Kronig-Penney model was used to show that broadening of the absorption is a better metric of quantum mechanical coupling than shifting. However, broadening is complicated by grain growth of the QDs that can occur during thermal annealing or from QD–QD necking after ligand removal, resulting in both larger QDs and larger size distribution. Difficulty in separating true quantum mechanical coupling from dielectric effects has been noted,²³ and similar phenomena are expected to contribute to the absorption spectra of the films studied here. Overall, red-shifting and broadening may be viewed as a signature of electronic coupling but not a quantitative measure due to uncertainty about the how much each of the various effects contributes.

Displayed in Figure 3 are normalized and offset-subtracted CPTG decay curves for two different QD sizes and a variety of surface treatments. 2.8 nm OA-capped QDs (solution or film) exhibit fast CPTG decay rate constants of 10 ps⁻¹, slowing to 7 ps⁻¹ for 3.0 nm QDs. The slowing is caused by the change of QD size and thus reduction in splitting between fine structure levels. Pyridine-treated QDs exhibit decays that are similar to, or slightly faster than, those of OA-capped QDs. Decays measured for solution samples (Figure S4) were identical to within error, suggesting that without QD–QD coupling the nature of the ligand does not significantly affect the CPTG decay.

Treatments with Na₂S reduce the decay rate constant by about 20% compared with untreated QDs, while subsequent Cd(NO₃)₂ treatment reduces the k_{CPTG} by about 1 order of

magnitude with respect to untreated films. The MCC treatments In₂Se₃ and In₂Te₃ both greatly reduce k_{CPTG} to 2.8 and 0.47 ps⁻¹, respectively, for the 2.8 nm QD size. It should be noted that CPTG signals become increasingly difficult to measure under conditions of intense diffuse scattering of k_3 , which is inevitable in some treated films, particularly after exchange with inorganic salts. A larger background signal contributes noise to the decay and can produce interference with the CPTG signal, obscuring the true kinetics. This effect is mostly responsible for the varying signal-to-noise ratios apparent in Figure 3.

CPTG decay kinetics after 0.1 ps are essentially mono-exponential after subtraction of an offset, and all fits assume one decay constant. Table 1 contains average rate constants (k_{CPTG})

Table 1. Parameters Measured for 2.8 nm Diameter CdSe QDs from Steady-State Absorption (First Two Columns), Transient Grating Spectroscopy (Next Three Columns), and Pump–Probe Spectroscopy (Last Column)^a

treatment	E_{ex} (eV)	Γ_{ex} (eV)	k_{CPTG} (ps ⁻¹)	Δ_{CPTG}	$d_{\text{ex}}/d_{\text{QD}}$	NN
OA solution	2.290	0.12	11.2	0.04	1.00	0
OA film	2.290	0.12	10.5	0.05	1.01	0
Pyr	2.290	0.13	9.7	0.06	1.03	b
Pyr 150C 2 min	2.245	0.20	3.8	0.38	1.33	b
Pyr 150C 5 min	2.225	0.22	4.0	0.20	1.29	b
Pyr 175C 2 min	2.215	0.23	0.72	0.40	1.98	b
[In ₂ Se ₃] ²⁻	2.225	0.21	2.8	0.24	1.42	6
In ₂ Te ₃	2.160	0.30	0.47	0.28	2.21	6
Na ₂ S	2.225	0.21	8.5	0.15	1.07	2
Na ₂ S/Cd(NO ₃) ₂	2.180	0.25	1.8	0.19	1.58	b

^a E_{ex} and Γ_{ex} are the peak position and width, respectively, of the first exciton band estimated from the steady-state absorption spectra.

^bThese films had fast trapping kinetics that complicated TA analysis.

and the magnitude of the average offset Δ_{CPTG} resulting from the fits to CPTG decays obtained on at least five locations for each film. The fast decay rate represents the most facile conversion of the initially excited exciton of ± 1 angular momentum projection, which has the largest oscillator strength from the ground state, to one of opposite sign ∓ 1 via a direct or two-step pathway (Figure 4a). Past work has shown the two-step process to be dominant, with the limiting step being a hole flip to the ∓ 2 exciton. Slower decays, often seen as an offset in >10 ps time windows, represent a separate pathway involving states with $F = 0$, which are normally only a minor contributor in small, isolated CdSe QDs²⁴ but become significant upon exciton shape and size distortion.

The effect of thermal annealing of pyridine-treated arrays on the CPTG signal is shown in Figure 3c,d. Initial heating at 150 °C produces a 2-fold reduction in k_{CPTG} , while continued heating at that temperature has only a minor effect. Raising the annealing temperature to 175 or 200 °C decreases the rate by another factor of 3. For the smaller QDs, 200 °C annealing produced a film that changed greatly in optical quality and texture, suggesting significant sintering. This was often accompanied by a low energy absorption tail that extended to the bulk band gap energy. The larger QDs were able to withstand annealing at 200 °C without dramatic changes in film quality. Samples that have been significantly sintered and lose most of the oscillator strength in the lowest exciton band show weak signals dominated by scattering and lack a clear decay in

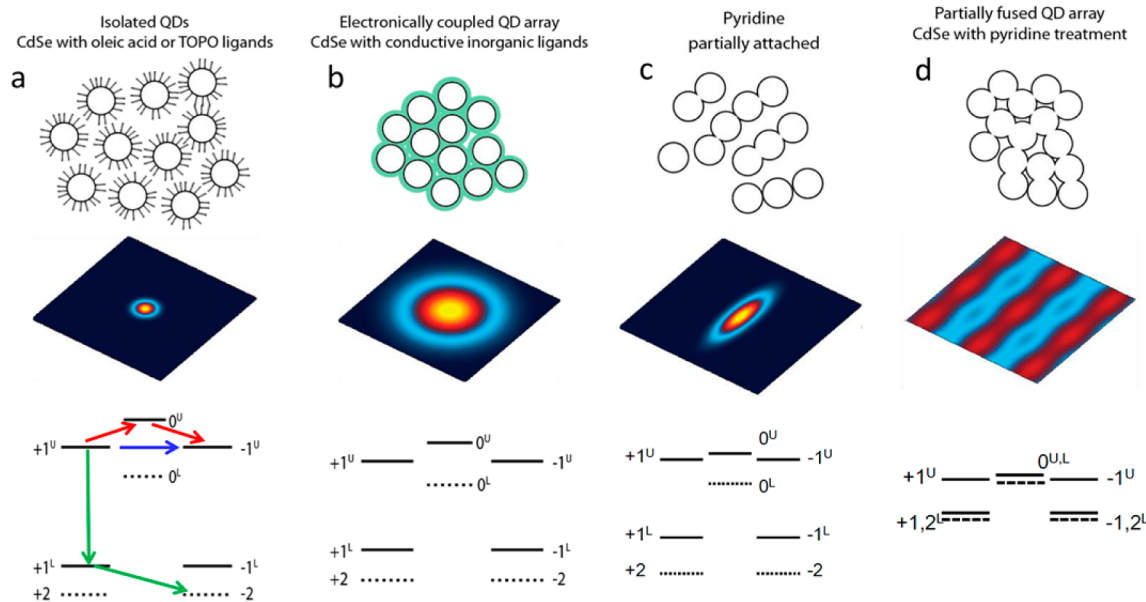


Figure 4. Schematic diagram of the effect of QD film environment on the exciton wave function and fine structure. (a–d) Inter-QD environment and associated 2D wave function projection with associated fine structure levels for each regime. (d) The sample under significant annealing, approaching the bulk situation.

the 0.1–10 ps time window, suggesting that a quantum-confined exciton with fine structure levels as shown in Figure 4a–c is not formed. In this sense, the technique only measures the simultaneous presence of quantum confinement and exciton delocalization.

If k_{CPTG} from coupled QDs are compared with those of isolated QDs, an effective exciton size can be determined.¹⁶ Whether or not such a comparison is truly quantitative may depend on the exact electronic interaction that gives rise to the fine structure splitting and if it changes in a fundamental way upon the introduction of QD–QD coupling; however, as long as the mechanism depends on quantum confinement (i.e., electron–hole overlap)²⁵ the comparison provides a practical means by which to compare degrees of coupling. For unannealed OA- or pyridine-capped QDs in solution or film we find exciton size (d_{ex}) to be equal to the QD size (d_{QD}), to within uncertainty. For other treatments the effective exciton size is larger, reaching $2.2 \times d_{\text{QD}}$ for 2.8 nm In₂Te₃-capped QDs. It is interesting that this treatment produces the largest size exciton, even in the absence of annealing. [In₂Se₄]²⁻, of similar length to In₂Te₃ and shown to produce very high mobilities in FET measurements, also produced a larger exciton, but only about $1.4 \times d_{\text{QD}}$. Significant annealing of the pyridine-treated QDs nearly doubled d_{ex} but further increases could not be achieved before other film properties significantly changed, suggesting loss of quantum confinement. Na₂S treated QDs, ostensibly the closest together physically, exhibited less than 10% expansion of the exciton. However, secondary treatment with Cd²⁺ did increase the size to nearly $1.6 \times d_{\text{QD}}$, suggesting that surface electrostatic properties or bridging of the QDs plays a role in exciton delocalization.²⁰

Δ_{CPTG} (here considered to be any decay slower than 0.05 ps⁻¹), shown in Table 1, should be related to the relative influence of the upper spin flip pathway through the 0^U state. In CdSe nanorods the 0^U energy depends not only on the nanorod diameter but also on its length, falling below the ±1^U levels for aspect ratios significantly greater than 1, even as the diameter remains constant. In this sense, Δ_{CPTG} could be an

indicator of preferential elongation of the exciton wave function along a chain of aligned QDs,²⁶ if Δ_{CPTG} and k_{CPTG} are not correlated in a manner that would be expected for isotropically delocalized excitons.²⁷ Although Δ_{CPTG} is found to be more variable than k_{CPTG} , values are similar to previous measurements for CdSe rods with aspect ratios from 1 to 3.²⁸ For most samples, Δ_{CPTG} and $1/k_{\text{CPTG}}$ grow equally as QDs are more strongly coupled, suggesting that the exciton expansion is approximately spherical. Deviations toward an elongated exciton may be found in pyridine-treated films, where Δ_{CPTG} rises noticeably without a significant decrease in k_{CPTG} , and evidence for chain formation is observed (Figure 1c and Figure S5).

Pump–probe transient absorption (TA) spectroscopy (Figure 5) was performed at increasing photon fluences to investigate biexciton decay characteristics for the various films. Unlike CPTG, TA will not report on coherent delocalization but may reveal how subsequent incoherent exciton dynamics are affected by strong electronic coupling. For isolated QDs above band gap photons are absorbed by the ensemble following Poisson statistics, giving the number of excitons per QD as $\langle N_{\text{eh}} \rangle = \sigma_a J_0$, where σ_a is the per-QD absorption cross section and J_0 is the photon fluence. When $\langle N_{\text{eh}} \rangle$ begins to exceed ~0.3, the number of excited QDs that have absorbed more than one photon exceeds 10%, and evidence of biexciton decay becomes apparent. When the biexciton decay is fast compared to the single exciton decay ($\tau_2 \ll \tau_1$) the total decay kinetics can be modeled as a sum of exponentials ($\Delta A = \sum_i^n a_i \exp(-\tau_i)$) whose amplitudes (a_i) are dictated by Poisson statistics and thus are determined by σ_a and J_0 . TA dynamics are well-behaved at the lowest fluences, for which single exponential kinetics are observed with lifetimes ranging from 2 ns for the [In₂Se₄]²⁻ treated films to 7 ns for the OA-capped QDs. A faster component ($\tau_2 = 15–30$ ps) rises with increasing fluence consistent with Auger recombination, similar in both OA-capped QDs in film and solution. In contrast, strongly annealed pyridine-capped QDs show evidence of a < 100 ps decay at all fluences (Figure S1) and cannot be subject to the Auger

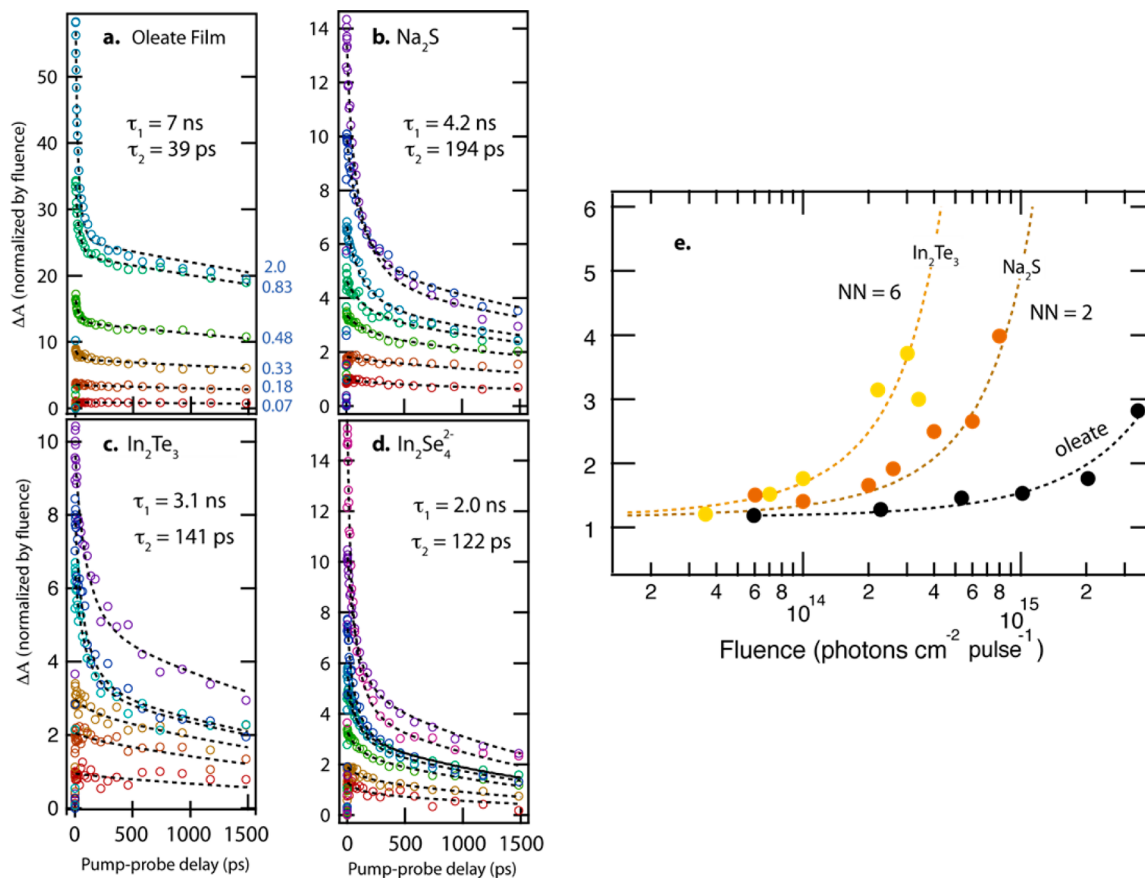


Figure 5. Transient absorption data for the various 2.8 nm CdSe QD films taken at a variety of increasing pump-photon fluences. Treatments are: (a) OA, (b) Na₂S, (c) In₂Te₃, and (d) [In₂Se₄]²⁻, with values $\langle N_{eh} \rangle$ shown in the lower right of panel a. The single and biexciton lifetimes extracted from a global fit are noted on each graph. Panel e shows the ratio of early to late times as a function of pump fluence for OA, Na₂S, and In₂Te₃ films. The curve for [In₂Se₄]²⁻ was very similar to that of In₂Te₃ and is excluded for clarity.

analysis described here. Although it may be possible to determine decay schemes in such films,²⁹ for our present purposes, only samples without clear evidence of a fluence-independent sub-ns decay are studied further by TA. Bulk-like Auger recombination³⁰ was also considered but not found to provide a satisfactory fit to the TA data.

Biexciton decay is governed by an Auger process, the rate of which has been conclusively shown in isolated QDs to be inversely proportional to QD volume.⁴ However, in electronically coupled QD films a new Auger process not available in isolated QDs is possible, leading to an onset of fast decay at much lower J_0 corresponding to $\langle N_{eh} \rangle$ calculated for individual QDs of <0.1. Concomitant with the lower threshold for biexponential kinetics in strongly coupled QD films is the slowing of the faster decay time to as long as ~200 ps, about 1 order of magnitude larger than for uncoupled QDs, similar to observations in coupled PbSe QD films.³¹ The slower Auger process may result from reduced Coulomb interactions between carriers as the time-averaged distance between them increases after delocalization. Then, the d^3 scaling of the Auger decay time predicts a biexciton size of about twice d_{ex} very similar to that inferred from CPTG measurements.

In Figure 5e we plot the ratio of early time to late time TA amplitude (R) as a function of J_0 . In the case of isolated QDs, $R = \sigma_a J_0 / [1 - \exp(-\sigma_a J_0)]$, which at low fluences is 1. At higher fluences $R = \sigma_a J_0$,³² which exceeds 1 at a lower effective $\langle N_{eh} \rangle$ in coupled QD films than in isolated QDs. This could result from a higher σ_a , which is known to increase under close QD

packing,³³ but at the lowest exciton absorption the enhancement should be only minor. Instead, strong coupling hastens the rates of energy and charge transfer, allowing electrons and holes to interact and undergo Auger recombination over distances larger than d_{QD} . This interaction volume is essentially the distance over which carriers and/or excitons can move during the excited state lifetime. We can modify R to account for carriers that interact on neighboring QDs by dividing by the probability of not finding an excited carrier within an interaction sphere. This is done by calculating the probability of finding two QDs within a sphere of radius r that have absorbed a photon: $P'(r) = \sum_{i=0}^{NN} NN! (1 - P_0)^i P_0^{NN-i} / [i!(NN - i)!]$, where $P_0 = \exp(-\langle N_{eh} \rangle)$ is the probability of exciting zero QDs and NN is the number of interacting nearest neighbors within r such that $R_{\text{films}} = R_{\text{sol}} / [1 - P'(r)]$. We modeled our data using R to extract σ_a for the OA film (Figure 5e, black dotted line) with NN = 0. The dashed brown and tan lines that reproduce the Na₂S and In₂Te₃ data use σ_a determined from the OA-capped QDs and only differ by setting NN = 2 for Na₂S and NN = 6 for In₂Te₃. There appears to be a correlation between d_{ex} from CPTG and NN from TA, suggesting that coherent delocalization affects the subsequent incoherent process of exciton migration and Auger annihilation. The fact that τ_2 , NN, and d_{ex} are not perfectly correlated may stem from the onset of other excited state pathways occurring on a picosecond time scale, such as localization due to trapping or interactions between excitons and pre-existing trapped charges.^{34–36} Such events are less likely to affect k_{CPTG} ; thus

d_{ex} measured by CPTG remains a measure of the effective initial exciton size with all treatments.

Without question, the center-to-center distance between QDs plays a large role in exciton delocalization and can account for the general trends observed as ligands significantly shorter than OA are employed; however, at short ranges ligand length does not solely dictate d_{ex} . One consideration is to what degree disorder of spacing and orientation impedes delocalization. Order was not specifically measured in these samples, but all films are drop-casted from solution, which provides opportunity for short-range, but not likely long-range order. Another source of disorder is the energetic mismatch due to QD size polydispersity. The 1S exciton energies vary by as much as 100 meV, indicating that some QD nearest-neighbors on the high energy side of the distribution may inhibit delocalization. Ligand electronic states may also act either as tunneling/activation barriers or efficient molecular wires, depending on their electronic structure. An energetic resonance between empty orbitals in In_2Te_3 and CdSe $\langle 1\text{S}_{\text{e}}1\text{S}_{\text{h}} \rangle$ exciton states (Figure 1d), lacking with many of the organic ligands and simple anions, may facilitate delocalization. Similarly, the static charge distribution at the surface of a QD may result in localization, explaining the compensatory effect of Cd^{2+} treatment after OA exchange with S^{2-} .

One intriguing question is how our CPTG results relate to measurements of transport. Although the two experiments investigate processes occurring over different length/time scales, the large gate bias employed in FET measurements creates a “trap-free” regime, which CPTG also probes by time scale discrimination. Literature reports suggest pyridine-treated CdSe QD films exhibit small mobilities μ ($< 10^{-5} \text{ cm}^2 \text{ V}^{-1} \text{ s}^{-1}$),³⁷ while extensive annealing at 350 °C produces much higher values ($\sim 1 \text{ cm}^2 \text{ V}^{-1} \text{ s}^{-1}$).³⁸ $[\text{In}_2\text{Se}_4]^{2-}$ treatments of CdSe QDs produce $\mu > 10 \text{ cm}^2 \text{ V}^{-1} \text{ s}^{-1}$ mentioned earlier,¹¹ although to our knowledge, treatments involving In_2Te_3 have not yet been tested for FET mobility. K_2S treated films have produced $\mu_e \sim 0.01 \text{ cm}^2 \text{ V}^{-1} \text{ s}^{-1}$,⁶ and when followed by a Cd^{2+} treatment, the mobility increases to $1.3 \text{ cm}^2 \text{ V}^{-1} \text{ s}^{-1}$.²⁰ While ongoing work in our laboratory is aimed at measuring FET mobilities under the exact conditions as used for CPTG, the trends between literature values of μ and d_{ex} measured here suggest that, for very high mobilities ($\gg 1 \text{ cm}^2 \text{ V}^{-1} \text{ s}^{-1}$), an effective exciton size significantly greater than $1 \times d_{\text{QD}}$ may be necessary.

In summary, we have measured the exciton size in electronically coupled CdSe QDs using a method that selectively monitors coherent exciton expansion in the initial period after photoexcitation. We have found that the effective exciton size can be larger than two QD diameters and that it is roughly spherical, suggesting that all of the QD nearest neighbors are involved in the coherence. While making a connection between the ultrafast “snapshot” provided by CPTG and events at later times is challenging, general trends suggest that the coherent expansion influences both subsequent photophysics and transport. The technique can be applied and the conclusions generalized to other nanomaterial systems in which nominally quantum-confined excited state properties are modified by electronic coupling with the surroundings.

ASSOCIATED CONTENT

Supporting Information

Femtosecond spectroscopy methods and pulse properties, ligand synthesis and film preparation methods, additional

TEM images of CdSe QDs, and further information about transient absorption data analysis. This material is available free of charge via the Internet at <http://pubs.acs.org>.

AUTHOR INFORMATION

Corresponding Author

*E-mail: justin.johnson@nrel.gov.

Notes

The authors declare no competing financial interest.

ACKNOWLEDGMENTS

J.N.S., M.C.B., and J.C.J. were supported by the Department of Energy, Basic Energy Sciences, Division of Chemical Sciences, Biosciences, and Geosciences under contract No. DE-AC36-08GO28308 with NREL for spectroscopy and data analysis. R.W.C. and J.M.L. were funded for QD film preparation, characterization, and treatments by the DOE SunShot program under award no. DE-EE0005312.

REFERENCES

- (1) Efros, A. L.; Rosen, M. *Annu. Rev. Mater. Sci.* **2000**, *30*, 475–521.
- (2) Efros, A. L.; Rosen, M.; Kuno, M.; Nirmal, M.; Norris, D. J.; Bawendi, M. *Phys. Rev. B* **1996**, *54*, 4843–4856.
- (3) Nozik, A. J.; Beard, M. C.; Luther, J. M.; Law, M.; Ellingson, R. J.; Johnson, J. C. *Chem. Rev.* **2010**, *110*, 6873–6890.
- (4) Klimov, V. I.; Mikhailovsky, A. A.; McBranch, D. W.; Leatherdale, C. A.; Bawendi, M. G. *Science* **2000**, *287*, 1011–1013.
- (5) Nozik, A. J. *Annu. Rev. Phys. Chem.* **2001**, *52*, 193–231.
- (6) Chung, D. S.; Lee, J. S.; Huang, J.; Nag, A.; Ithurria, S.; Talapin, D. V. *Nano Lett.* **2012**, *12*, 1813–1820.
- (7) Luther, J. M.; Law, M.; Song, Q.; Perkins, C. L.; Beard, M. C.; Nozik, A. J. *ACS Nano* **2008**, *2*, 271–280.
- (8) Nag, A.; Kovalenko, M. V.; Lee, J. S.; Liu, W. Y.; Spokoyny, B.; Talapin, D. V. *J. Am. Chem. Soc.* **2011**, *133*, 10612–10620.
- (9) Kovalenko, M. V.; Scheele, M.; Talapin, D. V. *Science* **2009**, *324*, 1417–1420.
- (10) Talgorn, E.; Gao, Y. N.; Aerts, M.; Kunneman, L. T.; Schins, J. M.; Savenije, T. J.; van Huis, M. A.; van der Zant, H. S. J.; Houtepen, A. J.; Siebbeles, L. D. A. *Nat. Nanotechnol.* **2011**, *6*, 733–739.
- (11) Lee, J. S.; Kovalenko, M. V.; Huang, J.; Chung, D. S.; Talapin, D. V. *Nat. Nanotechnol.* **2011**, *6*, 348–352.
- (12) Guyot-Sionnest, P. *J. Phys. Chem. Lett.* **2012**, *3*, 1169–1175.
- (13) Wang, L.; Beljon, D. *J. Phys. Chem. Lett.* **2013**, *1888–1894*.
- (14) Shabaev, A.; Efros, A. L.; Efros, A. submitted 2013.
- (15) Johnson, J. C.; Gerth, K. A.; Song, Q.; Murphy, J. E.; Nozik, A. J. *Nano Lett.* **2008**, *8*, 1374–1381.
- (16) Kim, J.; Wong, C. Y.; Scholes, G. D. *Acc. Chem. Res.* **2009**, *42*, 1037–1046.
- (17) Scholes, G. D.; Kim, J.; Wong, C. Y.; Huxter, V. M.; Nair, P. S.; Fritz, K. P.; Kumar, S. *Nano Lett.* **2006**, *6*, 1765–1771.
- (18) Scholes, G. D.; Kim, J.; Wong, C. Y. *Phys. Rev. B* **2006**, *73*.
- (19) Klimov, V. I.; Schwarz, C. J.; McBranch, D. W.; Leatherdale, C. A.; Bawendi, M. G. *Phys. Rev. B* **1999**, *60*, R2177–R2180.
- (20) Nag, A.; Chung, D. S.; Dolzhnikov, D. S.; Dimitrijevic, N. M.; Chattopadhyay, S.; Shibata, T.; Talapin, D. V. *J. Am. Chem. Soc.* **2012**, *134*, 13604–13615.
- (21) Micic, O. I.; Nozik, A. J.; Lifshitz, E.; Rajh, T.; Poluektov, O. G.; Thurnauer, M. C. *J. Phys. Chem. B* **2002**, *106*, 4390–4395.
- (22) Dollefeld, H.; Weller, H.; Eychmuller, A. *J. Phys. Chem. B* **2002**, *106*, S604–S608.
- (23) Foos, E. E. *J. Phys. Chem. Lett.* **2013**, *4*, 625–632.
- (24) Wong, C. Y.; Kim, J.; Nair, P. S.; Nagy, M. C.; Scholes, G. D. *J. Phys. Chem. C* **2009**, *113*, 795–811.
- (25) Scholes, G. D.; Rumbles, G. *Nat. Mater.* **2006**, *5*, 683–696.
- (26) Peng, X. G.; Manna, L.; Yang, W. D.; Wickham, J.; Scher, E.; Kadavanich, A.; Alivisatos, A. P. *Nature* **2000**, *404*, 59–61.

- (27) Smith, E. R.; Luther, J. M.; Johnson, J. C. *Nano Lett.* **2011**, *11*, 4923–4931.
- (28) Kim, J.; Wong, C. Y.; Nair, P. S.; Fritz, K. P.; Kumar, S.; Scholes, G. D. *J. Phys. Chem. B* **2006**, *110*, 25371–25382.
- (29) Tyagi, P.; Kambhampati, P. *J. Chem. Phys.* **2011**, *134*, 094706.
- (30) Ghanassi, M.; Schanneklein, M. C.; Hache, F.; Ekimov, A. I.; Ricard, D.; Flytzanis, C. *Appl. Phys. Lett.* **1993**, *62*, 78–80.
- (31) Beard, M. C.; Midgett, A. G.; Law, M.; Semonin, O. E.; Ellingson, R. J.; Nozik, A. J. *Nano Lett.* **2009**, *9*, 836–845.
- (32) Beard, M. C.; Knutson, K. P.; Yu, P. R.; Luther, J. M.; Song, Q.; Metzger, W. K.; Ellingson, R. J.; Nozik, A. J. *Nano Lett.* **2007**, *7*, 2506–2512.
- (33) Geiregat, P.; Justo, Y.; Abe, S.; Flamee, S.; Hens, Z. *ACS Nano* **2013**, *7*, 987–993.
- (34) Kraus, R. M.; Lagoudakis, P. G.; Muller, J.; Rogach, A. L.; Lupton, J. M.; Feldmann, J.; Talapin, D. V.; Weller, H. *J. Phys. Chem. B* **2005**, *109*, 18214–18217.
- (35) Klimov, V. I.; McBranch, D. W. *Phys. Rev. B* **1997**, *55*, 13173–13179.
- (36) Cohn, A. W.; Janssen, N.; Mayer, J. M.; Gamelin, D. R. *J. Phys. Chem. C* **2012**, *116*, 20633–20642.
- (37) Webber, D. H.; Brutchey, R. L. *J. Am. Chem. Soc.* **2012**, *134*, 1085–1092.
- (38) Ridley, B. A.; Nivi, B.; Jacobson, J. M. *Science* **1999**, *286*, 746–749.